Clinics of Oncology

Research Article ISSN: 2640-1037 | Volume 6

Flavin-Containing Dimethylaniline Monooxygenase 5 Drives Malignancies in Hepatocellular Carcinoma by Blocking IQGAP1 Ubiquitination via Increasing its SUMOylation

Li Z[1,*], Dong W[2], Zhang W[1], Xu Y[3], Zhang S[1], Jiang J[1], Chen Y[1], Zhao X[1], Dong H[2*], Wang J[1*] and Zhao RC[1,4,*]

[1]School of Life Sciences, Shanghai University, China

[2]Department of Pathology, Eastern Hepatobiliary Surgery Hospital, the Second Military Medical University, China

[3]School of Medicine, Shanghai University, Shanghai, China

[4]Institute of Basic Medical Sciences Chinese Academy of Medical Sciences, School of Basic Medicine Peking Union Medical College, China

[*]Corresponding author:

Robert Chunhua Zhao,
School of Life Sciences, Shanghai University, 807A Rm, 19# Bldg., 381 Nanchen Road, Baoshan District, Shanghai 200444, China,
E-mail: zhaochunhua@vip.163.com

Jiao Wang,
School of Life Sciences, Shanghai University, 410 Rm, 19# Bldg., 381 Nanchen Road, Baoshan District, Shanghai 200444, China,
E-mail: jo717@shu.edu.cn

Hui Dong,
Department of Pathology, Eastern Hepatobiliary Surgery Hospital, and Key Laboratory of Signaling Regulation and Targeting Therapy of Liver Cancer, the Second Military Medical University, 225 Changhai Road, Shanghai 200438, China,
E-mail: huidongwh@126.com

Zhe Li,
School of Life Sciences, Shanghai University, 437 Rm, 19# Bldg., 381 Nanchen Road, Baoshan District, Shanghai 200444, China,
E-mail: zhe_li0913@shu.edu.cn/ lzshanghai@163.com

Received: 25 Dec 2022
Accepted: 06 Feb 2023
Published: 15 Feb 2023
J Short Name: COO

Citation:

Zhao RC, Wang J, Dong H,Li Z, Flavin-Containing Dimethylaniline Monooxygenase 5 Drives Malignancies in Hepatocellular Carcinoma by Blocking IQGAP1 Ubiquitination via Increasing its SUMOylation. Clin Onco. 2023; 6(19): 1-21

Keywords:

Flavin Containing Dimethylaniline Monooxygenase 5; Oncogene; Metastasis; IQ motif-containing GTPase-activating protein; Hepatocellular carcinoma

Abbreviations:

HCC: Hepatocellular Carcinoma; FMO5: Flavin Containing Dimethylaniline Monooxygenase 5; IQGAP1: IQ Motif-Containing GTPase-Activating Protein 1; GDSC: Genomics of Drug Sensitivity in Cancer; TCGA: The Cancer Genome Atlas; UGT: UDP Glucoronosyl Transferases; TMA: Tissue Microarray; HIPAA Health Insurance Portability and Accountability Act 1996; TCGA-LIHC: The Cancer Genome Atlas liver cancer; GEO: Gene Expression Omnibus; IRS: Immunoreactivity Score; H&E: Hematoxylin and Eosin; CTRP: Genomics of Therapeutics Response Portal; qPCR: quantitative Real-Time Polymerase Chain Reaction; TCGA-LIHC: The Cancer Genome Atlas-Liver Hepatocellular Carcinoma; GEPIA: Gene Expression Profiling Interactive Analysis; OS: Overall Survival; PFS: Progression Free Survival; DFS: Disease Free Survival; DSS: Disease Special Survival; IHC: Immunohistochemical; DFS: Disease-Free Survival; TCPA: The Cancer Proteome Atlas; CHX: Cycloheximide

1. Abstract

Hepatic microsomes play an important role in drug metabolism, but the potential biological functions of hepatic microsome-containing proteins in Hepatocellular Carcinoma (HCC) remain unclear. Here, we used HCC and corresponding adjacent Non-Tumor (NT) tissues to isolate hepatic microsomes and then performed RNA high-throughput sequencing. After screening, flavin-containing dimethylaniline monooxygenase (FMO5) showed a sig-

nificantly high expression level and was associated with poor prognosis in patients with HCC. In vitro and in vivo assays revealed that the overexpression of FMO5 significantly enhanced cell invasion and metastasis. Then, we constructed an FMO5-GST fusion protein for pulldown assays with mass spectrometry, which showed that FMO5 can directly bind with IQ Motif-Containing GTPase-Activating Protein 1 (IQGAP1) in HCC cells. Mechanistically, higher levels of FMO5 promote the binding of FMO5 to the poly proline protein-protein domain of IQGAP1, which opens its secondary structure and increases the level of SUMOylation at the C-terminus thereby reducing its ubiquitin-mediated degradation. In summary, our findings demonstrate that FMO5 acts as an oncogene in HCC cells by directly binding to IQGAP1 and affecting its post-translational modifications. FMO5 may serve as a candidate prognostic biomarker and target novel therapies for patients with HCC.

2. Introduction

Hepatocellular Carcinoma (HCC) is the third leading cause of cancer-related death worldwide [1]. Although the major risk factors for HCC are well known, many patients often have viral infections, chronic liver inflammation, or metabolic syndrome; more than 50% of patients with HCC have advanced cancer at initial diagnosis, and 70% of patients experience recurrence within 5 years of initial treatment [2]. Therefore, the molecular mechanisms underlying HCC require further investigation.

Hepatic microsomes are generally defined as fractions obtained by differential centrifugation techniques that are composed solely of smooth and rough membrane vesicles from the disrupted endoplasmic reticulum [3, 4]. Studies have suggested that hepatic microsomes contain several microsomal enzymes, including flavin monooxygenases, NADPH cytochrome c reductase, cytochrome P450, UDP glucuronosyl transferases (UGT), glutathione-S-transferases, and epoxide hydrolases [5, 6]. Microsomal-derived proteins have been well-characterized in terms of their general chemical composition, enzymatic composition, and morphological characteristics [7]. However, there remains a gap in the study of the biological functions of microsomal-derived proteins in hepatocarcinogenesis.

In this study, we isolated microsomes from human HCC and the corresponding adjacent Non-Tumor (NT) tissues and performed RNA sequencing. Flavin-containing dimethylaniline monooxygenase 5 (FMO5) showed a significantly higher expression level and was identified as an oncogene in HCC. Flavin-containing monooxygenases (FMOs) have been known for decades as conserved amine oxidases and phosphorous oxidases that catalyze the oxygenation of a diverse range of nucleophilic drugs and dietary constituents requiring NADPH and oxygen [8-10]. Six forms of human FMO (FMO1–FMO6) family members have been identified [11-13], and as FMO6 is unable to encode a functional protein it is considered a pseudogene [14]. The distribution of FMOs in the genome is different, with FMO1, FMO2, FMO3, FMO4, and FMO6 clustered in the region q24.3 on Chromosome 1. FMO5 is located in the region Chr1q21.1, which has identified a significant copy number gain region in HCC (http://genome.ucsc.edu/, Human GRCh38/hg38) [15, 16]. Recent studies suggested the importance of FMO5 in drug metabolism, aging, diurnal rhythm, and alcoholic fatty liver disease [17-22]. However, the biological functions and specific molecular mechanisms of FMO5 in HCC remain unclear.

Here, we demonstrate that overexpression of FMO5 accelerates metastatic and proliferative abilities in vitro and in vivo. Mechanistically, we found that FMO5 exerted its oncogenic effect by directly binding to IQ motif-containing GTPase-Activating Protein 1 (IQGAP1). In normal tissues, IQGAP1 exists in its inactive form via intramolecular interactions. However, in HCC, with a higher FMO5 protein level, FMO5 directly binds to the WW domain (a polyproline protein-protein domain) of IQGAP1, which fully opens the IQGAP1 structure. The Lysine at 1445 site of IQGPA1 is then SUMOylated by SUMO1 and SUMOylated IQGAP1 reduces its ubiquitinated degradation. Therefore, FMO5 overexpression increases the protein stability of IQGAP1, which in turn activates downstream signaling pathways and promotes malignant progression in HCC.

3. Materials and Methods

3.1. Human Clinical Samples and Ethical Statement

Cohort 1 included 160 paired RNA samples of patients with HCC and corresponding adjacent NTs were obtained from the Department of Pathology of Eastern Hepatobiliary Surgery Hospital, Second Military Medical University (Shanghai, China). Cohort 2 contained 80 fresh paired HCC and corresponding adjacent NT liver tissues were obtained from the Department of Pathology of Eastern Hepatobiliary Surgery Hospital. Cohort 3 comprised a Tissue Microarray (TMA) obtained from the Department of Pathology of the Eastern Hepatobiliary Surgery Hospital and was constructed from 90 paired histologically confirmed HCC samples and normal liver tissues. All human tissues were collected under HIPAA (Health Insurance Portability and Accountability Act 1996) approved protocols. This study was approved by the Institutional Ethics Committee of Shanghai University and the Eastern Hepatobiliary Surgery Hospital. All human-related experiments were performed in accordance with the Declaration of Helsinki. In addition, we used the dataset from The Cancer Genome Atlas Liver Cancer (TCGA-LIHC) to analyze the mRNA levels of FMO5 and IQGAP1. We also used a dataset of 50 paired HCC and corresponding NT liver tissues from the Gene Expression Omnibus, GSE77314) dataset to analyze FMO5 transcripts in HCC. Clinical information for Cohort 2 is provided in Supplementary Table S1.

Supplementary Table 1: Correlation of the expression of FMO5 in liver cancer with clinicopathologic factors

Characteristics	No. of patients	FMO5 (low)	FMO5 (High)	*P* -value
Sex				0.1389
male	41	17	24	
female	39	19	20	
Age (yr)				0.5027
< 60	32	12	22	
≥ 60	48	25	23	
Tumor size (cm)				**0.0075**
<5	27	7	20	
≥5	53	14	39	
Differentiation grade				**0.002**
Well and moderately	52	13	39	
Poorly	28	6	22	
Tumor stage				**0.0036**
I-II	36	12	24	
III-IV	44	9	35	

3.2. Microsome Isolation of Liver Tissue

We used the Microsome Isolation Kit (catalog number: K249-50, Bio Vision, USA) to isolate microsomes from human liver tissues. Briefly, frozen liver tissue (300 mg) was placed in a pre-chilled Dounce homogenizer. Then 2 mL of cold homogenization buffer was added to the sample and the tissue sample was gently homogenized about 20 strokes on ice. Then an additional 2 mL homogenization buffer was added to fully suspend the homogenate. The homogenate was then transferred to a microcentrifuge tube, vortexed for 30 s, and the centrifuged at 10,000 × g for 15 min at 4°C. The thin floating lipid layer was gently discarded and the supernatant was not aspirated. The supernatant was transferred to a new, pre-chilled microcentrifuge tube and centrifuged at the speed of 30,000 × g for 40 min at 4°C. After centrifugation, any floating lipids and the supernatant were discarded, and a light beige/pink opalescent (microsomal) pellet was obtained. The microsomal pellet was resuspended in 500 µL of ice-cold storage buffer for RNA isolation.

3.3. Cell Lines and Cell Culture

Human cell lines (Huh-7) were obtained from the Cell Bank of the Chinese Science Academy (Shanghai, China). HEK293T cells were obtained from American Type Culture Collection (ATCC, USA). All cells were cultured at 37°C in a humidified incubator with 5% CO2 in Dulbecco's Modified Eagle's medium (Invitrogen Life Technologies) supplemented with 10% Fetal Bovine Serum (FBS) (Gibco). Cryopreserved human primary hepatocytes were purchased from Lonza (catalog number: HUCPI; USA). We used thawing medium (Catalog number: MCHT50, Lonza) to recover the human primary hepatocytes and cultured them in the medium prepared with the Hepatocyte Culture Medium Bullet Kit (Catalog number: CC-3198, Lonza). All cell lines were routinely tested by quantitative reverse transcriptase polymerase chain reaction (qRT-PCR) and showed negative results for mycoplasma (the sequences of the PCR primers for test mycoplasma: Myco_F1: ACGCGTAGAACCTTACCCAC, Myco_R1: ACGACAACCATGCACCATCT; Myco_F2: GTGCTGGATATCCCGGGCTAAGC Myco_R2: AGGCGAACCGTTCACTCCCC).

3.4. Immunohistochemistry Assay and Evaluation of TMA Slide Immunostaining

TMA specimens were blocked by proteolytic digestion and using peroxidase, followed by incubation with 1:50 anti-FMO5 monoclonal antibody (ab189516; Abcam, Cambridge, MA, USA) at 4°C overnight. After washing with PBS, peroxidase-labeled antibodies and substrate chromogens were used to visualize the staining of the target proteins. TMA slides were scanned using a Scan Scope and analyzed using Image Scope v11 software (Aperio Technologies, USA). We also used Dako Envision Systems (Dako Diagnostics AG, Switzerland) to analyze the Immunohistochemistry (IHC) data. Two independent experienced pathologists who were blinded to the clinicopathological data and clinical outcomes of the patients evaluated the immunostaining scores of the samples. Each sample was assessed for staining intensity as follows: nonsignificant brown, weak brown, moderate brown, and strong brown staining intensities were scored as 0, 1, 2, and 3, respectively. The immunoreactivity score (IRS) was determined by multiplying the intensity and extent of the positivity scores of the stained cells. The final scores were compared between the two pathologists [23]. The samples were classified as high (based on an IRS value >4) or low (based on an IRS value ≤4) levels per FMO5 protein expression.

3.5. siRNA, shRNA, Plasmid Construction, and Lentiviral Transfection

siRNAs targeting FMO5 and negative controls were purchased from RiboBio (Guangzhou, China). Full-length FMO5 and IQGAP1 were cloned into the lentivirus expression vector Pwpxl (Addgene, Shanghai). The details of siRNA, shRNA, and plasmid contraction were previously described [24]. For transient transfection, siRNA transfection was performed using the Lipofectamine iMax kit (Invitrogen Life Technologies, USA). Additionally, target plasmids psPAX2 and pMD2.G were co-transfected into HEK293T cells for lentivirus packaging using Lipofectamine 3000 (Invitrogen Life Technologies, USA). Supernatants containing lentivirus particles were collected 48 h after transfection. The cells were infected with lentiviruses in the presence of 6 µg/mL Polybrene (Sigma-Aldrich). All sequences are listed in Supplementary Table 2.

Supplementary Table 2: Sequences for the primers and siRNA

Primer name	Primer (5'→3')
ENST00000254090.9-F-qPCR	AATCCCAGATCATTATCCCAAC
ENST00000254090.9-R-qPCR	CTCTCTTTCCAGTGAATCCCTC
ENST00000369272.7-F-qPCR	GAAGCAGCCTGATTTTGCCACT
ENST00000369272.7-R-qPCR	CTCTACAGCCAGATCCCCTCCA
ENST00000441068.6-F-qPCR	CTGCGTAGAAGAAGGCTTGGAA
ENST00000441068.6-R-qPCR	GAGGTAGATGAGCATTGGTGTG
ENST00000478432.1-F-qPCR	CTGCGTAGAAGAAGGCTTGGAA
ENST00000478432.1-R-qPCR	TGGGATAATGATCTGGGATTGG
ENST00000527849.5-F-qPCR	TGCTGTGATTGGGGGAGGAGTG
ENST00000527849.5-R-qPCR	AAGTTGGGATAATGATCTGGGA
ENST00000533174.5-F-qPCR	GATTGGGGGAGGAGTGAGCGGG
ENST00000533174.5-R-qPCR	TTAGAAGGTCAAATTCTTTGGC
ENST00000533848.2-F-qPCR	GAATAAAAACCTCTTCCTTCTT
ENST00000533848.2-R-qPCR	GAGCCCGCTCACTCCTCCCCCA
ENST00000619062.1-F-qPCR	AGTCGAGACTATAAGAACCCAG
ENST00000619062.1-R-qPCR	CGAGAAGAGAACAACACATCAG
ENST00000578284.5-F-qPCR	CTTCTCGACTTACACATTTTAT
ENST00000578284.5-R-qPCR	CACATTTCCTTTCACTTTCACC
IQGAP1-F-qPCR	AGAACGTGGCTTATGAGTACCT
IQGAP1-R-qPCR	CCAGTCGCCTTGTATCTGGT
FMO5-cds-F	ATGACTAAGAAAAGAATTGCTGTGA
FMO5-cds-R	TCACAGCAATTCTTTTCTTAGTCAT
IQGAP1-cds-F	ATGTCCGCCGCAGACGAGGTTGACG
IQGAP1-cds-R	TTACTTCCCGTAGAACTTTTTGTTG
GAPDH-F	ACAGTTGCCATGTAGACC
GAPDH-R	TTTTTGGTTGAGCACAGG
18S-F	GAGAAACGGCTACCACATCC
18S-R	CACCAGACTTGCCCTCCA
si-FMO5-1	ACCATGACTAAGAAAAGAATTGC
si-FMO5-2	GGCCAGTATTTACAAATCAGTGA

3.6. qRT-PCR and RNA Sequencing

Total RNA from cells or tissues was extracted using TRIzol reagent (Invitrogen Life Technologies). PrimeScript ™ RT Master Mix (Takara, Japan) was used for reverse transcription. qRT-PCR was performed using an Applied Biosystems 7900HT sequence detection system (Applied Biosystems) and TB Green® Premix Ex Taq™ II (Takara) kit. All reactions were conducted in triplicate. Primers were synthesized by Sangon Biotech (Beijing, China) and are listed in Supplementary Table 2. The details of RNA sequencing are described in our previous study [24]. Briefly, the Illumina HiSeq 4000 platform (Illumina) was used to sequence RNA samples to generate raw data. The R software package (The R Foundation for Statistical Computing) was used to select genes with significant differential expression based on fold changes of ≥2.0 and P≤ 0.05 between the different groups. KEGG pathway analysis and GSEA were used for the functional pathway analysis.

3.7. Immunocytochemistry

After cleaning the coverslips with ethanol, we seeded the HCC cells at a density of 1x105 cells per poly L-lysine-coated coverslip well and allowed them to grow overnight. The culture medium was then removed and the cells were fixed with 4% formaldehyde for 20 min at room temperature. The cells were washed twice with PBS and incubated with PBST (PBS with 0.1% Triton X-100) for 30 min. After washing three times with PBS, the cells were blocked with 5% goat serum for 1 h. After removing the blocking buffer, the cells were incubated with 1:200 anti-FMO5 monoclonal antibody (ab189516; Abcam) at 4°C overnight. The next day, the primary antibody was removed and the cells were washed with PBST three times for 5 min each. The cells were then incubated with the secondary antibody for 1 h in the dark and washed three times with PBST for 5 min each. DAPI was used for nuclear labeling by incubation for 10-15 min followed by three 5 min washes

with PBS. A fluorescence mounting medium (S3023, Dako) was applied at the edges of the coverslip, and the samples were examined under a confocal microscope.

3.8. Migration and Invasion Assays

Cell migration and invasion assays were performed using a Transwell assay (Corning, USA) with (for invasion assay) or without (for migration assay) Matrigel (BD Biosciences) according to the manufacturer's instructions. Briefly, 4×104 cells for migration and 1×105 cells for invasion in serum-free medium were seeded in the upper chamber, and 800 μL of medium containing 10% FBS was placed in the lower chamber. After 24–48 h, the cells that migrated to the bottom of the membrane were fixed with 4% paraformaldehyde and stained with hematoxylin and eosin (H&E) (Beyotime Biotechnology, China). Five fields were randomly selected for counting analysis. The experiments were performed in triplicate.

3.9. Soft Agar Assay

We evaluated the capacity of cells for anchorage-independent growth in soft agar. pWPXL-FMO5 or negative control cells at 1,000 cells/mL in DMEM medium were suspended at a final concentration of 0.37% agar in the same medium and layered over a coating of 0.5% solid agar in 24-well tissue culture dishes using triplicate wells for each concentration. The plates were incubated in a 5% CO2 incubator at 37°C for up to 4 weeks. Colonies forming in soft agar were counted at weekly intervals in five microscopic fields per well.

3.10. Western Blot Assay

Total protein was extracted from the cells or tissues using RIPA lysis buffer (Beyotime Biotechnology, Shanghai, China). Electrophoresis was performed on a 10% sodium dodecyl sulfate-polyacrylamide gel electrophoresis (SDS-PAGE) gel, followed by transfer onto a PVDF membrane. After blocking with skim milk for 1 h at room temperature, membranes were incubated with primary antibodies overnight at 4°C, then incubated with secondary antibodies on the following day. Protein bands were analyzed using the Enhanced Chemiluminescence Plus Western Blotting Detection System (GE Healthcare). The antibodies used are listed in Supplementary Table 3.

Supplementary Table 3: Antibodies for western blot, Co-IP, and IHC

Protein Name	Company	Catalog Number	Dilutions in WB	Dilutions in RIP/IP	Dilutions in IHC
FMO5	NOVUS	#NBP1-86093	0.736111111	5μg	N/A
FMO5	Proteintech	13699-1-AP	N/A	N/A	0.180555556
IQGAP1	Cell Signaling Technology	#2293S	0.736111111	5μg	N/A
Ubiquitin Antibody	Proteintech	10201-2-AP	1.430555556	N/A	N/A
HA	Cell Signaling Technology	#3725	1.430555556	5μg	N/A
FLAG	Cell Signaling Technology	#8146	1.430555556	5μg	N/A
GAPDH	Proteintech	60004-1-IG	1.430555556	5μg	N/A
β-actin	Proteintech	60008-1-IG	1.430555556	N/A	N/A

3.11. GST-Pulldown Assay with Silver Staining

Escherichia coli (BL21) was transformed with pGEX-4T-3 or p-GEX-FMO5 and incubated with 0.2 mM isopropyl-β-D-1-Thiogalactopyranoside (IPTG) for 4 h. The GST fusion proteins were purified from bacterial lysates using GSH-Sepharose 4 B beads, according to the manufacturer's instructions (Amersham Biosciences Corp., USA). Tissue/cell lysates were prepared and centrifuged at 15,000 × g for 20 min. The Huh7 cell lysates were incubated with GST-FMO5-conjugated Sepharose beads for 2 h at 4°C. Following incubation, the supernatant was removed and the beads were washed with Tris-sucrose solution (10 mM Tris-HCl, 150 mM NaCl, 1% Triton X-100, pH 7.5) to remove any non-specific or non-covalently bound proteins. The beads were boiled in 1× sodium dodecyl sulfate (SDS) loading buffer. The eluate was separated by 7.5% SDS-PAGE and visualized using a silver staining kit (Beyotime Biotechnology, China) [16, 24].

3.12. Co-Immunoprecipitation (Co-IP) Assay

Cells transfected with the indicated plasmids were lysed in RIPA buffer, as in western blotting. After centrifugation, the supernatants were incubated with anti-FLAG or anti-HA Protein G Dynabeads (Life Technologies) overnight at 4°C with gentle rotation. The beads were washed three times with NT2 buffer (Life Technologies), and the proteins immunoprecipitated by beads were analyzed using SDS-PAGE.

3.13. In Vivo Animal Studies in Nude Mice

BALB/c male nude mice (6 weeks old) were purchased from the Shanghai Laboratory Animal Center of the Chinese Academy of Sciences and maintained in specific pathogen-free facilities. Mice were housed in single-sex cages (five mice per cage) at 22°C. In brief, for the tail vein injection mouse model, a total of 5 × 105 cells from each group were injected intravenously through the tail vein into BALB/c nude mice. About 7–8 weeks after injection, the mice were euthanized. Parts of the liver and lungs were fixed in 4% paraformaldehyde and embedded in paraffin, and the remaining tissues were left in liquid nitrogen for long-term storage. The number of metastatic foci in the liver and lungs was determined

using H&E staining (Beyotime Biotechnology) under a binocular microscope (Leica, Germany). All animals were euthanized to reduce pain. An anesthetic of 2 mL ZETAMINE™ (ketamine hydrochloride injection, NDC 13985-584-10, 100 mg/mL), and 1 mL of Xylazine sterile solution (NDC 59399-110-20, 20 mg/mL) in a 7 mL 0.9% Sodium Chloride Injection (NDC 63323-186-01) mixture was prepared to anesthetize the mice and was introduced into a container with a carbon dioxide concentration of 30% for euthanasia. All studies were supervised and approved by the Institutional Animal Care and Use Committee of Shanghai University.

3.14. Data Analysis and Statistics

All statistical analyses were performed using the GraphPad Prism 7. Wilcoxon and Mann–Whitney tests were used to analyze FMO5 mRNA levels in paired HCC and NT. The log-rank Mantel-Cox test was performed to analyze the correlation between the FMO5 mRNA levels and overall survival. Data are shown as mean ± standard deviation and were analyzed with one-way ANOVA or independent sample t-tests to examine the differences among different treatment groups. Statistical significance was set at $P < 0.05$.

4. Results

4.1. FMO5 is Significantly Upregulated in HCC Tissues

To explore the differentially expressed genes and long non-coding RNAs (lncRNAs) derived from the hepatic microsomes of HCC tissues, we first performed RNA sequencing of three fresh HCC tissue samples and used the corresponding adjacent NTs as controls. Through clustering analysis of the raw data, we identified upregulated genes in the microsomes (Figure 1A, B). The results showed the five most upregulated genes and lncRNAs (univariate Cox analysis, $P < 0.0001$ and log2 fold change >12.5) (Figure 1C, D). Among them, FMO5, a drug metabolism-related enzyme enriched in hepatic microsomes, showed significantly high expression in HCC tissues. This suggests that FMO5 plays an important role in malignant HCC progression. We also evaluated the correlation between FMO5 mRNA levels and drug sensitivity using the Genomics of Therapeutics Response Portal (CTRP) and Genomics of Drug Sensitivity in Cancer (GDSC) databases. The results showed a strong association between FMO5 mRNA levels and multiple drugs in a variety of tumors (Figure S1A, B). Therefore, FMO5 was selected for further study to determine characteristics and biological functions in HCC.

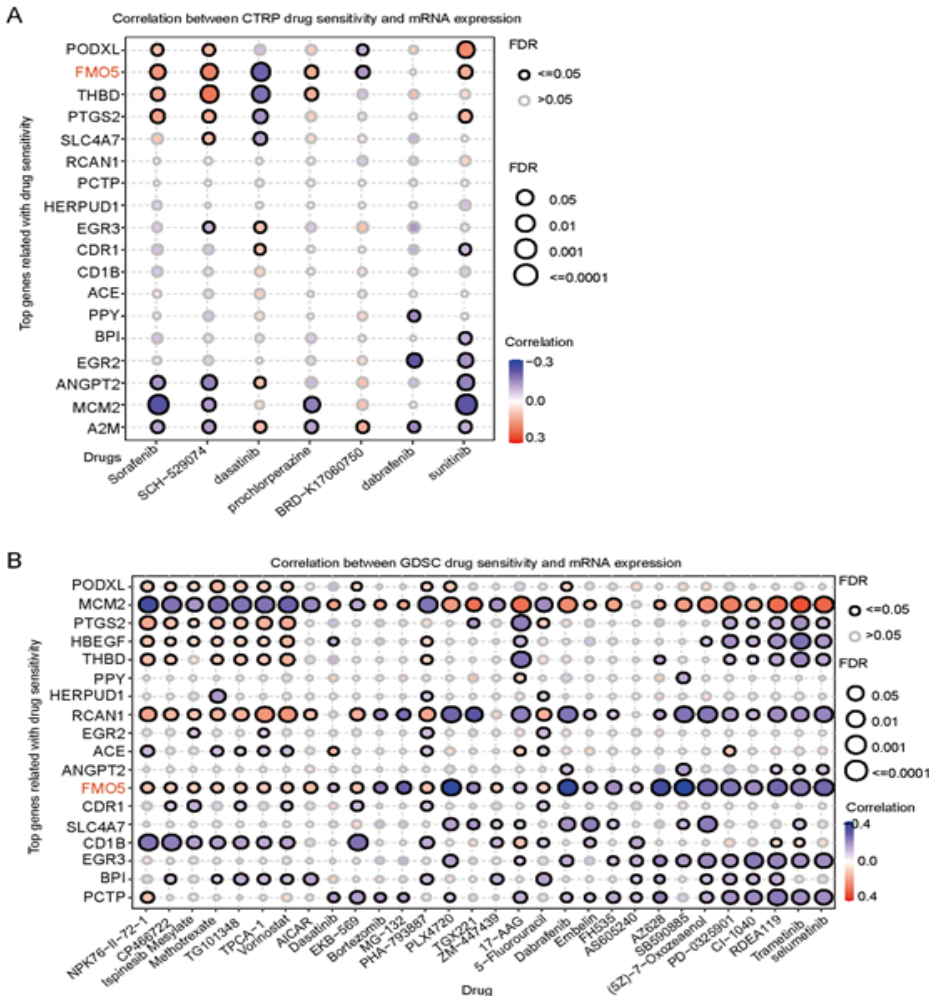

Figure S1: Correlation analysis of FMO5 with multiple drugs in CTRP and GDSC database.

(A): The Correlation of top genes with CTRG drug sensitivity at mRNA levels; (B): The Correlation of top genes with GDSC drug sensitivity at mRNA levels.

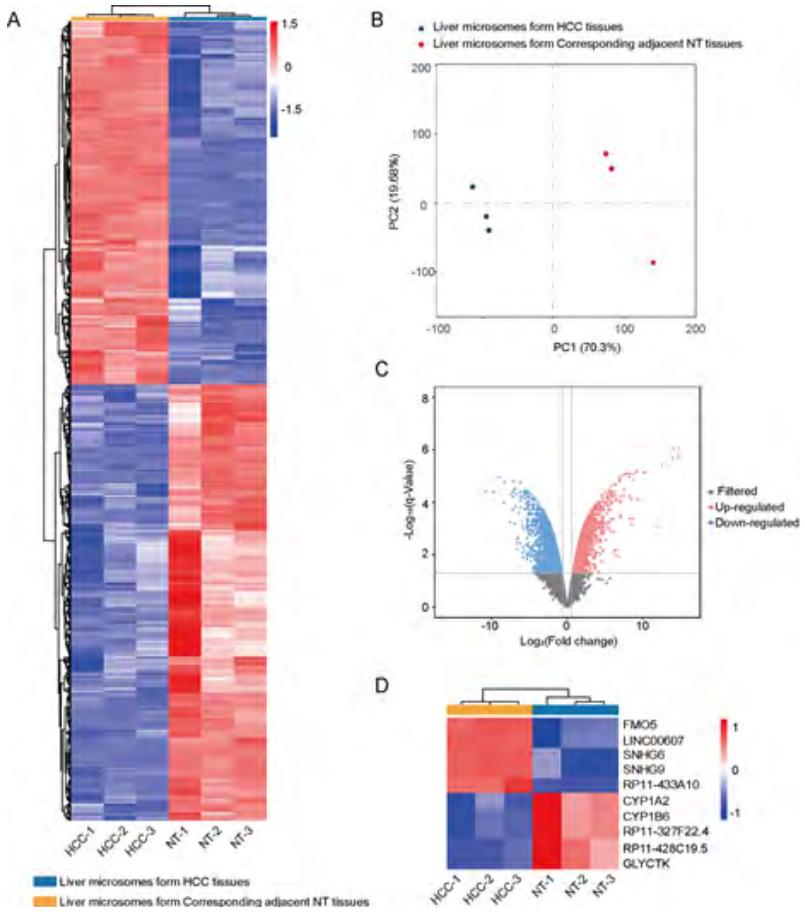

Figure 1: Screened FMO5 in three paired HCC tissues by RNA sequencing.

(A): Heat map showed clustering analysis of RNA-seq data by three HCC and corresponding adjacent NT tissues. Each row represents a gene and each column represents a sample. Red represents upregulated genes and blue represents downregulated genes. (B, C): Scatter plot (B) and volcano plot (C) results of reliability of RNA sequence. (D): Heat map showed clustering analysis of the genes with the most significant changes in mRNA levels. Red represents upregulated genes and blue represents downregulated genes.

4.2. FMO5-ENST00000254090.9 is the Predominant Transcript in HCC Tissues

Before analyzing the biological functions of FMO5, we must fully understand its basic characteristics in HCC. First, a combined analysis from the University of California, Santa Cruz (UCSC) Genome Browser (http://www.genome.ucsc.edu/) and Ensemble (https://useast.ensembl.org/index.html) databases revealed that FMO5 was localized at the q21.1 locus of chromosome 1 and existed in nine transcripts (Figure 2A and Figure S2A). Isoform analysis with GEO sequencing data (GSE77314, 50 paired HCC tissues) revealed that these eight isoforms showed different expression patterns. Among them, ENST00000254090.9 (FMO5-001) was significantly overexpressed in HCC (Figure S2B). We also analyzed the FMO5 transcripts in the NCBI database (https://www.ncbi.nlm.nih.gov/gene/2330), which identified isoform 1 (NM_001461, equivalent to ENST00000254090.9, encoding a 533-aa protein), isoform 2 (NM_001144829, equivalent to ENST00000441068.6, encoding a 464-aa protein), and isoform 3 (NM_001144830, equivalent to ENST00000369272.7, encoding a 285-aa protein). qRT-PCR revealed that ENST00000254090.9 (FMO5-001) was the predominant isoform in HCC tissues (Figure S2C). Therefore, we focused on FMO5- ENST00000254090.9, which encodes a 533-aa protein, in the subsequent experiments.

4.3. FMO5 is Upregulated in Human HCC Tissues with Copy Number Gains

In addition, data from The Cancer Genome Atlas HCC (TCGA-LIHC) and Gene Expression Profiling Interactive Analysis (GEPIA) database (http://gepia.cancer-pku.cn/) also showed that FMO5 mRNA was significantly overexpressed in liver cancer (Figure 2B). The mRNA expression level of ENST00000254090.9 was confirmed in 160 paired HCC and tumor-adjacent NTs (Cohort 1). Compared to NTs, FMO5 (ENST00000254090.9) was significantly upregulated in HCC tissues ($P < 0.0001$) (Figure 2C). Considering that FMO5 was localized in the significant copy number gain loci in the genome, we examined the copy number alterations of FMO5 in 80 paired DNA samples from HCC and NTs (Cohort 2). The results revealed that FMO5 had a significant copy number amplification with higher mRNA levels in HCC tissues (Figure 2D, E). Furthermore, the relationship between FMO5 mRNA levels and clinicopathological features was determined in Cohort 2. The results showed that higher mRNA levels of FMO5 were positively correlated with tumor differentiation, and the FMO5 mRNA level

in sorafenib-resistant HCC tumor tissues was higher than that in matched tumor tissues (Figure 2F). In addition, with its wide expression in different types of cancers, FMO5 was remarkably overexpressed in LIHC (Figure 3A). FMO5 was significantly associated with pathological stage (especially stage IV) in patients with liver cancer (TCGA data) (Figure 3B). Importantly, FMO5 mRNA levels are significantly associated with Overall Survival (OS), Progression-Free Survival (PFS), Disease-Free Survival (DFS), and Disease-Specific Survival (DSS) in various cancer types. In LIHC, a higher mRNA level of FMO5 was significantly correlated with DFS and DSS, but not with the OS of HCC patients (Figure 3C). These data suggest that FMO5 is a potential oncogene in HCC.

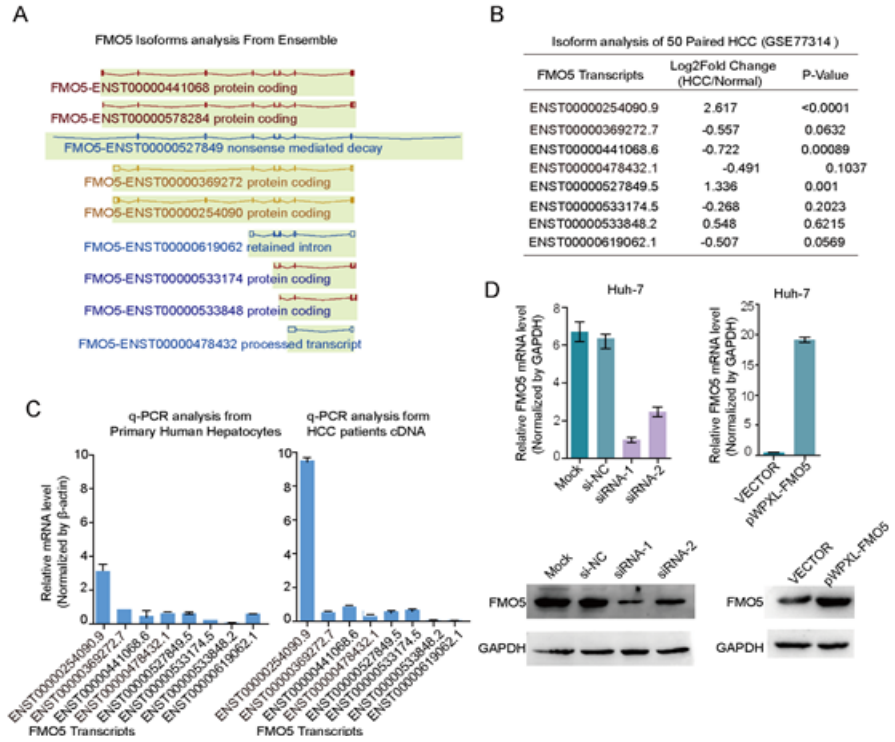

Figure S2: General information on FMO5 in HCC cells.

(A, B): Analysis of FMO5 isoforms (Human) in the public Ensemble database (https://useast.ensembl.org/index.html) and form the GEO (GSE77314) data; (C): qRT-PCR analysis of the basal expression levels of multiple isoforms of FMO5 in primary human hepatocytes and HCC tissues; (B): The subcellular location of FMO5 was determined by immunofluorescence assay in primary human hepatocytes; (C): The knockout and overexpression efficiency of FMO5 in Huh-7 cell lines at mRNA and protein level.

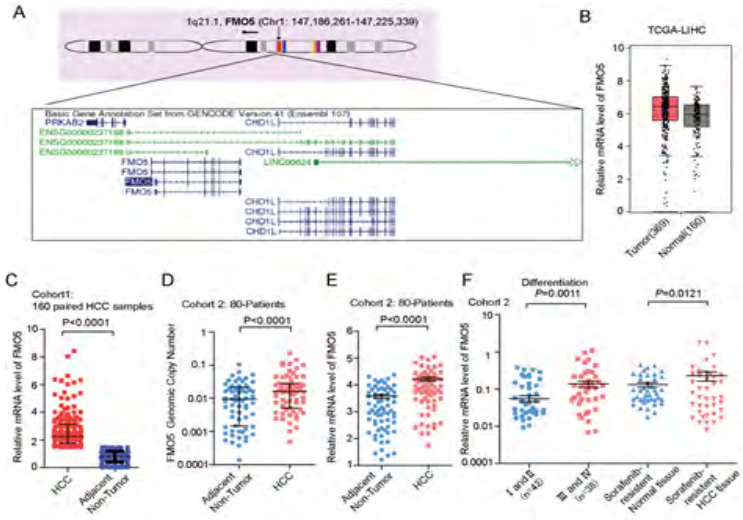

Figure 2: Detailed information for FMO5 in HCC.

(A): Graphical representation of the location and details of FMO5 on the human chromosome from UCSC Genome Browser (GRCh37/hg38). (B): The mRNA level of FMO5 was determined in TCGA-LIHC database. (C): The mRNA level of FMO5 was determined in 160 pairs of HCC tissues and adjacent normal tissues using qRT-PCR. (D): The copy number of FMO5 was determined in 80 pairs of HCC tissues and adjacent NTs using qRT-PCR. (E): The mRNA level of FMO5 was determined in cohort 2 using qRT-PCR. (F): Clinical significance of FMO5 in patients with HCC; high FMO5 mRNA level positively correlated with the patients at Ⅲ-Ⅳ stage and sorafenib resistant.

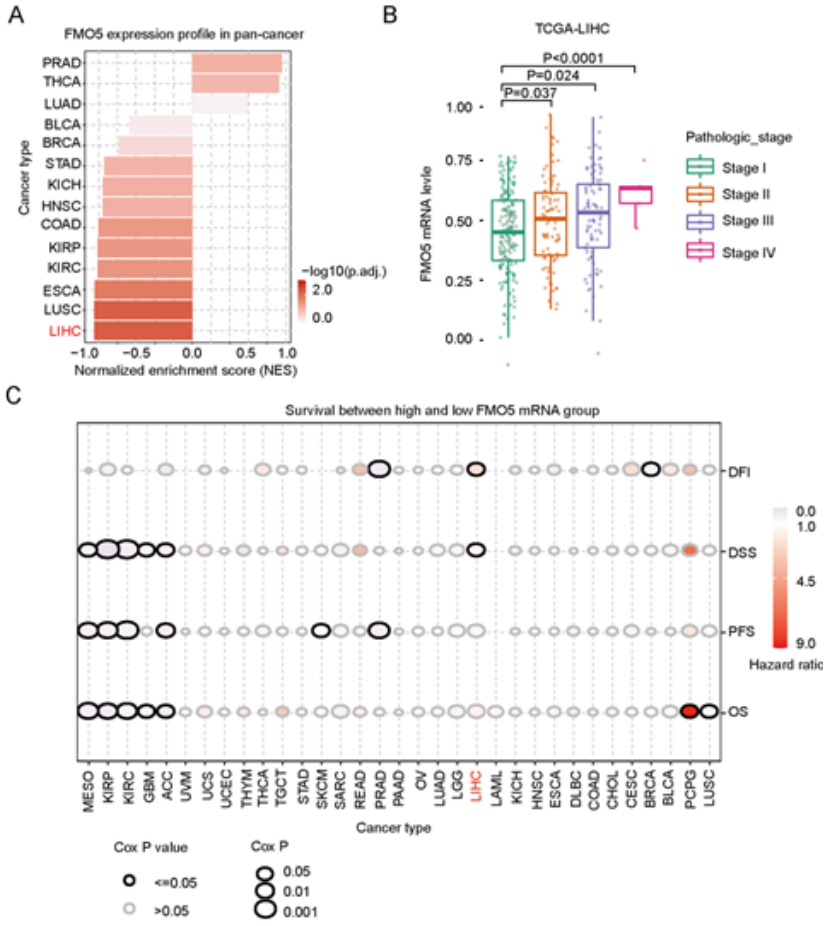

Figure 3: Clinical significance of FMO5 in pan-cancer.

(A): FMO5 expression profile in pan-cancer based on the normalized enrichment score (NES). (B): The correlation between mRNA level of FMO5 with pathologic stage of liver cancer patients in TCGA-LIHC database. (C): Clinical survival analysis of FMO5 based on the mRNA level in pan-cancer.

4.4. FMO5 was an Independent Prognostic Factor for Survival of Patients with HCC

To further determine the pathological significance of FMO5 in HCC, we performed IHC staining with 90 paired HCC and adjacent non-tumor tissues in Cohort 3 from Eastern Hepatobiliary Surgery Hospital. The staining of FMO5 was localized to the cytoplasm of HCC and normal cells (Figure 4A). Compared to NTs, FMO5 showed a significantly increased protein level in HCC tissues based on IHC scores ($P < 0.001$) (Figure 4B). The study further analyzed the correlation between FMO5 protein levels and the clinical or pathological characteristics of tissues in patients with HCC. Log-rank (Mantel-Cox) test results showed that patients with a higher protein level of FMO5 exhibited worse OS in HCC (Figure 4C). However, FMO5 expression did not correlate with prognosis in adjacent NTs (Figure 4D). Kaplan-Meier analysis also suggested that HCC patients with a higher protein level of FMO5 exhibited worse DFS (Figure 4E) and FMO5 was not associated with DFS in adjacent non-tumor tissues (Figure 4F). These findings indicate that FMO5 could serve as a valuable prognostic factor for the OS rate of patients with HCC.

4.5. FMO5 Acts as an Oncogene in Vitro and in Vivo

To further determine the role of FMO5 in HCC, we designed three independent siRNAs to knock down endogenous FMO5 after determining its primary localization in the cytoplasm (Figure S2B). We identified two siRNAs that effectively reduced the FMO5 mRNA levels (Figure S2C). To construct stably overexpressing FMO5 cell lines, we successfully cloned FMO5 into the pWPXL vector using the lentiviral packaging system. The results showed that the infection efficiency with lentivirus could reach more than 95%, and FMO5 was stably overexpressed at approximately 20-fold higher levels than that in the control group (Figure S2C). Silencing of FMO5 significantly inhibited the migration and invasion of Huh-7 cells (Figure 5A, B), whereas the numbers of migrating and invasive cells were both significantly increased in FMO5 overexpressed stable Huh-7 cells (Figure 5C, D). Soft agar colony formation assays indicated that overexpression of FMO5 significantly promoted the ability of HCC cells to grow in an anchorage-independent manner (Figure 5E), whereas FMO5 knockdown reduced HCC cell proliferation (Figure 5F). These investigations demonstrated the carcinogenic effects of FMO5 on HCC cells.

We further explored the effect of FMO5 on HCC tumorigenesis in vivo. We performed tail veil injections with FMO5-overexpressed Huh7 cells into BALB/c nude mice. Nine weeks later, the mice were sacrificed and metastatic foci in the lung and liver were de-

tected. There were significantly more metastatic loci in the lungs and livers of the FMO5-overexpressed group than those of the control group (Figure 5G, H). Collectively, these data indicate that FMO5 has a remarkable role in promoting the metastasis of HCC cells.

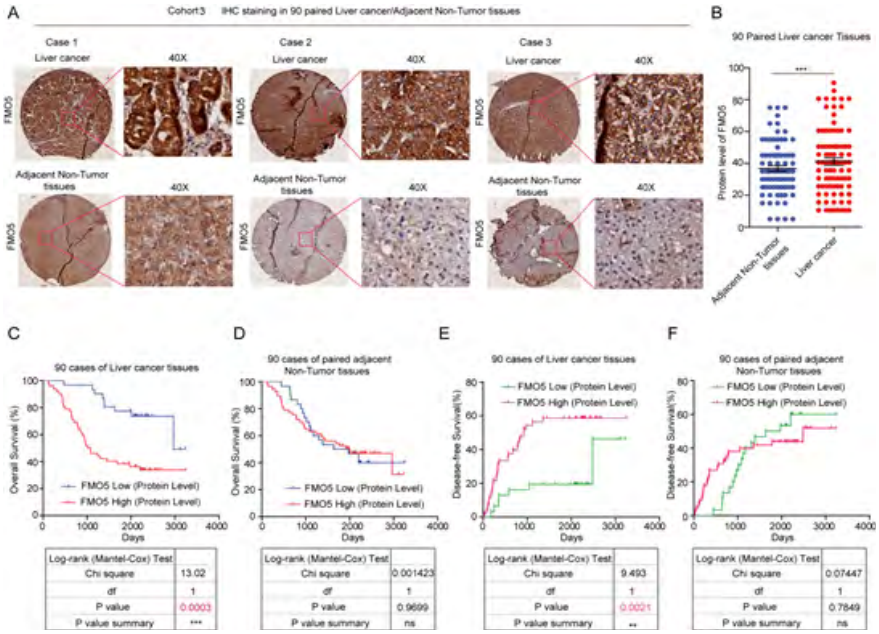

Figure 4: Immunohistochemical staining for FMO5 in liver cancer

(A, B): Representative images and statistical analysis by IHC staining of FMO5 in Cohort 3. (C, D): Kaplan-Meier overall survival analysis of FMO5 status in liver cancer tissues (C) and adjacent NTs (D) (Cohort 3, Gehan-Breslow-Wilcoxon test). (E, F): DFS curves of liver cancer patients with high and low FMO5 (Cohort 3).

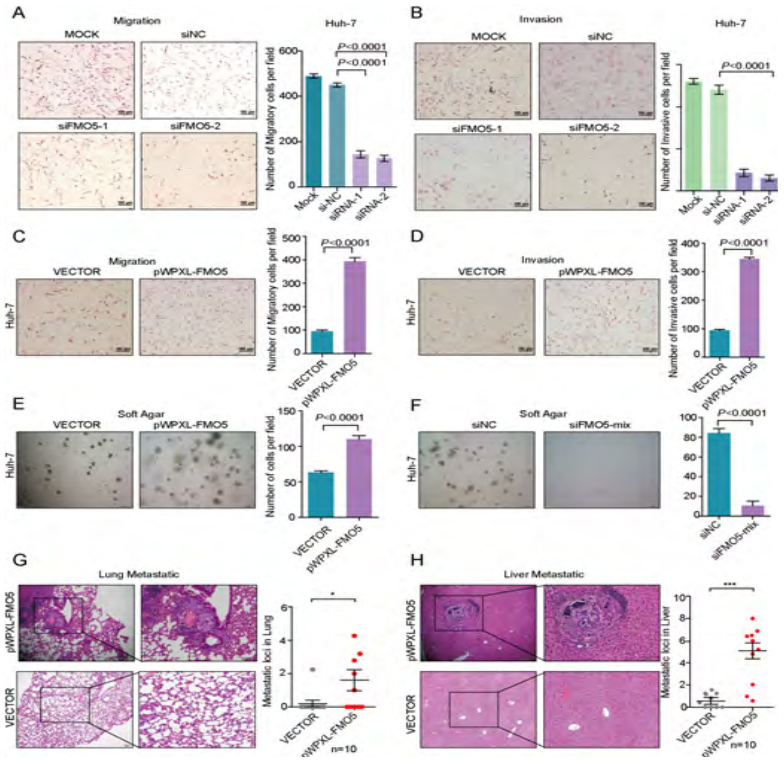

Figure 5: FMO5 promotes HCC cell invasion and metastasis in vitro and in vivo.

(A, B): Transwell migration (A) and invasion assays (B) in transfected with FMO5 siRNAs in Huh-7 cells. (C, D): Transwell migration (C) and invasion assays (D) in stable FMO5 overexpressed Huh-7 cells. (E, F): Soft agar assays were performed in Hun7 cells transfected with pwpxl-FMO5 (E), siRNAs (F) and their negative controls. (G, H): Statistical analysis and representative images of lung metastatic and liver metastatic by H&E staining of tail veil injection model for metastasis events in the vector and Lenti-FMO5 groups. Results from a representative experiment (n = 3) performed in triplicates are expressed as the means ± SEM (A-F).

4.6. Signaling Pathways Involved in the Regulation of FMO5 in HCC

To investigate the mechanism of FMO5 in HCC, we first analyzed the FMO5-related signaling pathways in pan-cancer using The Cancer Proteome Atlas (TCPA) database. The results showed that FMO5 was involved in the regulation of multiple signaling pathways and biological processes. In LIHC, the top five signaling pathways and biological processes included Apoptosis, EMT, Hormone AR, Hormone ER, and RAS_MAPK signaling pathways (Figure 6A). We also performed RNA sequencing of FMO5-overexpressed Huh7 cells to analyze the whole-genome profile affected by FMO5-mediated transcriptional regulation. We used Gene Set Enrichment Analysis (GSEA) to process the raw data and found that the top four signaling pathways and biological processes were EMT, G2M checkpoint, apoptosis, and KRAS_MAPK pathway, which was consistent with the signaling pathways in TCGA (Figure 6B, C and Supplementary Table 4). These signaling pathways are closely related to the malignant progression of tumors. To further validate this regulation, we selected four key regulator genes involved in these pathways to analyze whether these genes could respond to FMO5 overexpression (Figure 6D) or knockdown (Figure 6E). These results indicated that overexpression or knockdown of FMO5 can regulate the mRNAs levels of the top genes in these signaling pathways. These data suggested that FMO5 acts as an oncogene in HCC and is involved in the regulation of multiple signaling pathways; however, the specific mechanism of FMO5 requires further exploration.

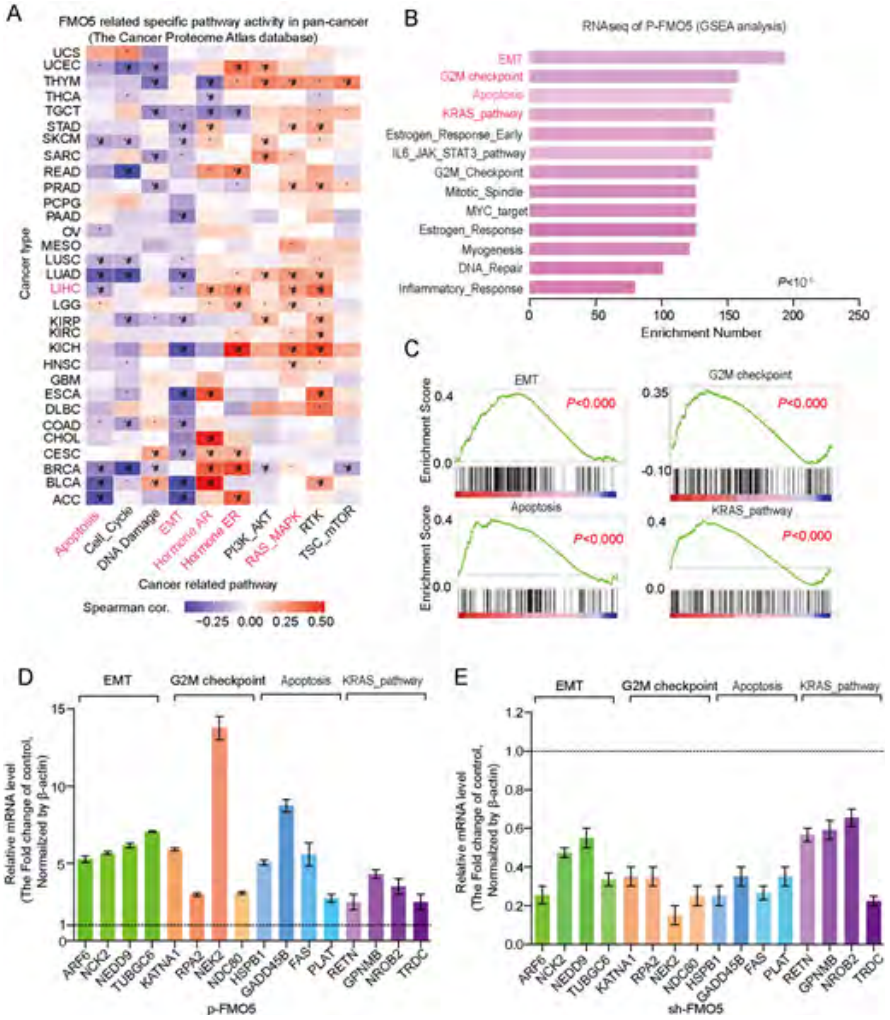

Figure 6: Analysis of the signaling pathways involved in FMO5.
(A): Analysis of FMO5 related signaling pathways in pan-cancer using TCPA database (B): GSEA analysis of RNA sequencing primary data after knockdown of FMO5. (C): Representative image of top four signaling pathways by GSEA analysis. (D, E): key genes of top four signaling pathways were verified by qRT-PCR when knockdown (D) or overexpressed (E) FMO5 in Hun-7 cells.

Supplementary Table 4: RNA-seq data of FMO5 overexpression in Huh7 cells

GeneID	Vector	Pwpxl-FMO5	Fold Change
PHGR1	0.081738027	4.684061909	57.30578648
OLFM4	0.032221204	1.500249894	46.56095151
SLC26A3	0.016301926	0.607226538	37.24876121
CLCA1	0.028200854	0.868638762	30.80186023
FABP1	0.134373551	3.304747278	24.59373336
MEP1A	0.015709328	0.382600042	24.35495925
AGR3	0.062312968	1.24981278	20.05702527
SERPINB5	0.01677054	0.288314698	17.19173594
SI	0.077645006	1.234738512	15.90235575
PIGR	0.283590265	4.500377499	15.86929472
REG4	0.481365672	6.551446624	13.61012429
ADH4	0.065094021	0.839309419	12.89380196
VIL1	0.042877734	0.542618916	12.65502785
MUC13	0.08105664	0.998678118	12.32074409
VILL	0.042056691	0.512144503	12.17747963
FCGBP	0.059696116	0.677059631	11.34177024
GAST	0.794424056	8.39368945	10.56575438
FABP2	0.056504132	0.593635853	10.50606085
KRT20	0.37617374	3.772463102	10.02851263
B3GNT3	0.020966942	0.210267244	10.02851263
KRT19	0.705122791	6.927019899	9.82384911
TMPRSS15	0.189196507	1.812656007	9.580811176
LGALS4	0.395271253	3.7461815	9.477495456
DMBT1	0.075156865	0.704016304	9.36729202
CEACAM5	0.064958126	0.604902428	9.312190302
ALDOB	0.285632884	2.618946732	9.168925836
CDH17	0.101104605	0.923399451	9.13310972
CEACAM6	0.051858237	0.470531367	9.073416192
HPGD	0.138768325	1.126565633	8.118319751
SULT1B1	0.032798604	0.26313697	8.022810107
GSTA1	0.274813032	2.165401829	7.87954564
EPCAM	0.29779382	2.249518015	7.553944581
JCHAIN	1.265802586	9.253220978	7.310161223
AOC1	0.029775064	0.213285435	7.163223309
CXCL14	0.02367956	0.169621978	7.163223309
TACSTD2	0.019852154	0.14220541	7.163223309
SLC44A4	0.088596077	0.609248144	6.876694377
MUC5AC	0.208645589	1.425594564	6.832613003
MS4A8	0.068991003	0.444778162	6.446900979
BTNL8	0.062816169	0.389970744	6.208126868
IGLL5	0.139842437	0.851464213	6.088739813
TSPAN8	0.431011732	2.558159009	5.935242171
LYZ	2.104834325	12.32413426	5.855156444
IL1R2	0.059153882	0.338985976	5.730578648
GSTP1	0.166588031	0.914868903	5.491804537
ST6GALNAC1	0.070263324	0.377483913	5.372417482
SLPI	0.156618837	0.78532699	5.014256317

ACTG2	0.090450413	0.453541556	5.014256317
TMEM45B	0.083567437	0.419028546	5.014256317
CAPN9	0.056367649	0.269182704	4.775482206
PPP1R1B	0.048633984	0.232250725	4.775482206
EBF3	0.042671921	0.198684523	4.656095151
FXYD3	0.318148693	1.458540886	4.584462918
SELENBP1	0.147905535	0.635688226	4.297933986
ARPP21	0.04078568	0.175294161	4.297933986
MLN	0.082460094	0.354408041	4.297933986
ST14	0.092316161	0.396768765	4.297933986
RPS4Y1	0.071528603	0.307425213	4.297933986
CREB3L1	0.052109133	0.223961613	4.297933986
SMIM24	0.245829114	1.056557305	4.297933986
TM4SF4	0.177715043	0.731982211	4.118853403
SPINT1	0.106906706	0.437598061	4.093270463
TFF1	3.218787123	12.98467017	4.034025758
CTSE	0.900769197	3.57133441	3.964760808
MUCL3	0.208843804	0.813821173	3.89679348
HHLA2	0.052519595	0.200645113	3.820385765
S100A14	0.498145626	1.86651022	3.746916808
SPARCL1	0.077943242	0.290328921	3.724876121
HMGCS2	0.115335453	0.413086802	3.581611655
LGALS9C	0.031674525	0.11344585	3.581611655
BCL2L14	0.114449272	0.393516334	3.438347189
AKR7A3	0.300231898	1.016660572	3.386251019
ADH1C	0.858343233	2.882111369	3.357760926
FBP1	0.12554785	0.404697279	3.223450489
MAL2	0.248433712	0.735562277	2.960798968
ANXA10	1.086936936	3.161576508	2.908702798
CD74	0.243226242	0.696913554	2.865289324
LAPTM5	0.062985713	0.180472291	2.865289324
MAN1A1	0.046542095	0.133356569	2.865289324
STC1	22.30852409	62.88718018	2.81897538
CA2	0.951388739	2.648118168	2.783423915
SPINT2	0.343269654	0.948439486	2.762957562
AADAC	0.198968875	0.529381723	2.660625801
TMPRSS2	0.100835461	0.268285429	2.660625801
GPX2	0.658517295	1.709951084	2.59666845
NDRG1	2.730271729	7.050789148	2.582449605
CDHR5	0.308153485	0.790975048	2.566821686
IQGAP2	0.207645918	0.514874105	2.479577299
CTXN1	6.923929443	17.05739381	2.463542408
CLDN7	0.291247509	0.695423648	2.387741103
CLDN18	0.808811708	1.899573402	2.348597806
PRR15L	0.245805995	0.572248051	2.328047576
RAB25	0.210236096	0.481909793	2.292231459
TPM4	58.24284414	130.3931766	2.238784499
CAPN8	0.287657401	0.643923187	2.238507284

RGS19	5.156525259	11.29107384	2.189667125
ACSL5	0.524719439	1.147387295	2.186668168
CASP7	6.424258467	14.00669272	2.18028163
DDR2	0.114843537	0.250085569	2.177619886
BLNK	0.209293333	0.449764465	2.148966993
GKN2	2.61714467	5.624157512	2.148966993
CYP1B1	13.14828557	28.24886361	2.148482664
AC026464.3	3.392852739	7.231851079	2.131495716
NES	3.44290922	7.290424641	2.117518695
KLHDC3	17.0406873	36.07696871	2.117107607
NTSR1	11.99566866	25.30901127	2.109845811
MUC1	0.951356146	1.988311267	2.089975742
SDCBP2	0.873225797	1.811825366	2.074864683
AMOTL1	13.62189275	28.1995801	2.070166064
WDR90	4.417553521	9.140248271	2.06907471
TCTEX1D2	3.967155129	8.190960509	2.064693777
MMP2	10.51719979	21.6448798	2.05804589
SCG2	21.61498022	44.02290856	2.036685119
PDK4	1.944683887	3.945333213	2.028778682
BICD2	6.448592344	13.06712612	2.026353261
G3BP2	29.99345339	60.74402374	2.025242741
STX12	6.366487035	12.81271205	2.012524644
HLA-DRA	0.182314114	0.36566788	2.005702527
REG1A	0.77701021	1.558451342	2.005702527
AKR1B10	4.491119014	8.915331167	1.985102407
OMA1	3.17062	6.289437902	1.98366184
TFF2	2.659757609	5.262101842	1.978414057
ZNF823	2.34999357	4.608523436	1.961079168
TBC1D9	3.324947648	6.502512555	1.955673665
OGFR	9.663861872	18.60823116	1.925548131
PRSS8	0.149591068	0.285747794	1.910192883
APOD	0.231433454	0.442082537	1.910192883
HRASLS2	0.18870248	0.360458133	1.910192883
VSIG2	0.744564108	1.403547098	1.885058766
ZNF680	4.556042991	8.584915187	1.884291962
ATP2A3	0.280460005	0.526495935	1.877258522
EREG	36.42651004	67.97964141	1.866213407
NPTX1	14.94391991	27.85823415	1.864185188
FAR1	0.08019315	0.149354775	1.86243806
HOXA2	0.468363405	0.872297831	1.86243806
NR2F1	8.627288058	16.03297319	1.858402442
STMN3	9.906224683	18.40138005	1.857557307
FJX1	32.6706893	60.66973832	1.857008212
MESD	9.785444999	18.14324254	1.854105004
CENPS	7.761714244	14.33866172	1.84735759
CYP2C18	0.270229026	0.497754221	1.841971708
NOLC1	27.83638261	51.12213151	1.836522088
LTBP1	2.947886517	5.40579057	1.833785167

DCBLD2	82.8622117	151.6531035	1.830184114
GKN1	33.02617943	60.37563029	1.828114282
A2M	0.105986075	0.193251398	1.823365933
U2AF1L5	0.2177716	0.397077316	1.823365933
B9D1	163.6466583	297.4577511	1.817683014
RNASE4	1.389059919	2.520703753	1.814683238
MED11	8.40439615	15.25131682	1.814683238
ETV1	4.86805735	8.829352454	1.813732218
AGR2	5.433739904	9.815388503	1.806378052
CHST14	3.774014393	6.809975961	1.804438259
TMEM141	26.59048099	47.97702052	1.804293068
IGFBP1	4.517595962	8.090137175	1.790805827
PLVAP	0.080993342	0.145043349	1.790805827
C8orf48	4.7156902	8.421748818	1.78589951
THRA	3.518308581	6.269872838	1.782070189
TANC2	6.004777684	10.66782012	1.776555383
SFN	4.31366244	7.648948899	1.773191344
TLE3	2.438512565	4.289839526	1.759203372
TSPAN1	1.907355589	3.353599804	1.758245721
ZNF100	3.468950474	6.063821851	1.748027796
IGF2	3.267486767	5.710760474	1.747753206
IL1R1	4.900467271	8.541764403	1.743051005
CCDC117	4.696521387	8.121117223	1.729177098
GPRIN1	4.178461128	7.224784518	1.729053902
WDR54	9.013560291	15.55263629	1.725470933
COMMD8	9.499694739	16.38624517	1.724923339
SPAG4	5.717611538	9.847974207	1.72239302
SPANXD	13.3447516	22.94194457	1.719173594
GALNT3	0.301657273	0.518601218	1.719173594
ZNF737	2.930252665	5.037613007	1.719173594
CD68	3.876941679	6.658014889	1.71733687
THBS3	4.040080775	6.916346757	1.711932791
TCTN2	5.630119766	9.624158045	1.709405562
ECE1	11.63377864	19.84050214	1.705422009
HIST1H2BD	7.157619781	12.20349513	1.704965548
RPIA	8.738449674	14.83476371	1.697642518
GPCPD1	3.608004276	6.124345782	1.697433072
ANGPTL4	6.507808558	11.03147683	1.695113913
GLI4	4.741261015	8.024944471	1.692575972
SPANXC	48.72262265	82.41497997	1.691513623
STK40	9.243781668	15.57925092	1.68537634
NOSTRIN	1.471735539	2.477457025	1.683357478
SEMA4B	12.16155345	20.46170372	1.682490959
ZBTB5	3.358961233	5.650358471	1.682174363
HELZ2	5.353668439	9.004882484	1.682002273
RFTN1	13.10020453	21.99683067	1.679121163
PAGR1	5.950595583	9.978675601	1.67692048
EXTL3	6.692519962	11.18330417	1.671015438
SIPA1L2	4.311442662	7.196231435	1.669100577

CCDC74A	6.442789391	10.74693193	1.668055757
PURG	0.795460261	1.325670982	1.666545831
PERP	74.70849931	124.3938078	1.665055635
RNPC3	4.746347114	7.896575446	1.663716382
ADAMTS15	5.528620082	9.193493271	1.662891125
ENSA	34.73103288	57.70604701	1.66151255
GANAB	52.75440467	87.6468809	1.661413515
SIAH2	4.135060851	6.853860075	1.657499205
KLF9	0.577204725	0.956136966	1.65649539
EMC6	20.33496222	33.60799052	1.652719595
SPRY4	9.929558108	16.37560828	1.64917795
TCF3	13.75740423	22.66889698	1.647759752
EIF4E3	0.093823326	0.154577809	1.647541361
MGAT5B	10.53558038	17.35631591	1.647400075
IFITM1	15.83040918	25.96394691	1.64013113
FAM3C	16.20880063	26.55403661	1.638248086
CXCL17	0.278760148	0.456416271	1.637308185
PTPRH	3.23829744	5.294699513	1.635025692
AC011530.1	9.86979349	16.05718248	1.626901565
AC253536.7	17.27748964	28.07498697	1.624945959
FOXQ1	1.657487176	2.693132737	1.624828702
ITPRID2	70.96398757	115.0949558	1.62187836
DDT	13.62763212	22.07565303	1.619918474
DYRK1B	1.970384555	3.191060164	1.619511357
ITPRIP	5.348094956	8.654040059	1.618153778
ZNF629	4.715546931	7.612524025	1.614345936
SDC4	57.42510858	92.68464261	1.614009009
CAMK2N1	0.159837032	0.257613379	1.611725245
FAM83E	0.193862568	0.312453195	1.611725245
WDR73	4.72182388	7.608731212	1.611396656
TRIM41	6.160891618	9.912984049	1.609017763
FAM72B	4.597115833	7.395334179	1.608689981
AKAP12	17.8674751	28.69833684	1.606177519
RABL2B	4.166512475	6.691851857	1.606103881
CABIN1	5.409756994	8.679933051	1.604495925
HILPDA	6.064006982	9.712504939	1.601664538
UBXN11	8.837066915	14.15131931	1.601359303

4.7. FMO5 Specifically Binds to IQGAP1 in HCC

To identify the specific binding protein of FMO5 in HCC, we performed an FMO5-GST tagged pulldown assay. A blank GST vector was used as a negative control, and specific bands were analyzed by mass spectrometry. After silver staining, we found a specific band located in the FMO5-GST group with a range of 130KD–250KD (Figure 7A, red arrow), which showed a significant difference from the control group. We obtained numerous proteins from this specific band using mass spectrometry analysis and screened for candidate proteins dependent on protein size as well as the number of unique peptides. Within this band the Ras GTPase-activating-like protein 1 (also named IQ motif-containing GTPase-activating protein 1, IQGAP1) had a high number of unique peptides, and the protein size also matched (Figure 7B). Moreover, we confirmed that IQGAP1 could specifically bind to FMO5 in HCC by Immunoprecipitation (IP) using western blotting (Figure 7C).

IQGAP1 is a multidomain scaffold protein that is ubiquitously overexpressed in various tumors [25-27]. Emerging evidence suggests that dysregulated IQGAP1 expression is associated with the oncogenesis of human cancers via modulation of several cellular functions, including the cell cycle, cell morphology, and motility, by linking elements of the cytoskeleton to cell adhesion and other signaling molecules [28, 29]. IQGAP1 facilitates space-time or-

ganization and the coordinated activation of structural and signaling molecules to regulate cell morphology and motility [26, 30-32]. IQGAP1 has also been reported in HCC tissues and is significantly upregulated and positively related to advanced TNM stage and poor clinical outcomes [33]. Our results confirmed that IQGAP1 was significantly overexpressed in HCC (Figure 7D). There was a strong positive correlation between FMO5 and IQGAP1 at the mRNA level in Cohort 1 (Figure 7E). High IQGAP1 levels were associated with poor OS of HCC (Figure 7F, $P < 0.0001$). These data indicated that FMO5 specifically binds to IQGAP1, and there was a remarkable positive correlation between the two at the mRNA level, suggesting that FMO5 probably exerts its oncogenic role by binding to IQGAP1 in HCC. However, the detailed molecular mechanisms require further investigation.

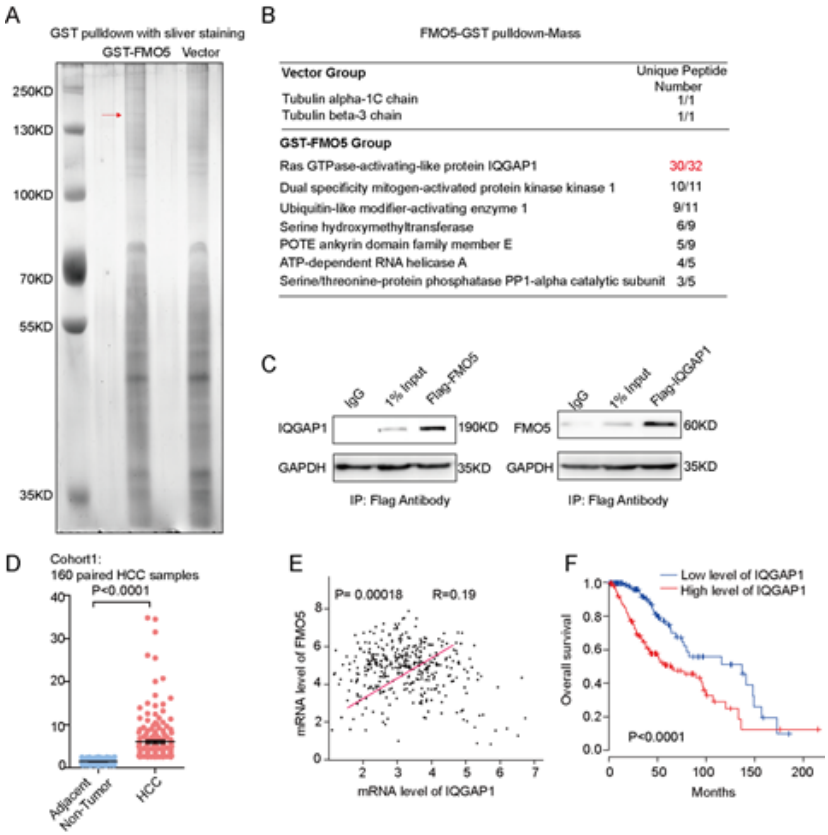

Figure 7: Identification of FMO5-interacting proteins

(A): GST- pulldown assay showed the proteins that bind with FMO5 in vitro by silver staining. (B): Mass spectrometry results showing the potential FMO5 binding proteins in red arrow. (C): Verified the interactions of IQGAP1 and FMO5 by western blot. (D): The mRNA level of FMO5 was determined in 160 pairs of HCC tissues and adjacent normal tissues using qRT-PCR. (E): Correlation between FMO5 and IQGAP1 at mRNA level in the Cohort 1. (F): Kaplan–Meier overall survival curves of Cohort 1 with high and low IQGAP1 mRNA levels.

4.8. FMO5 blocks IQGAP1 ubiquitination by increasing its SUMOylation in HCC

Considering that FMO5 interacts with IQGAP1 in HCC cells, we characterized the molecular consequences of this association. The results showed that FMO5 did not affect the mRNA level of IQGAP1(Figure S3A); however, the protein level of IQGAP1 was dramatically reduced when FMO5 was silenced and increased when FMO5 was overexpressed (Figure 8A, B). Hence, we further explored whether FMO5 affects the stability of IQGAP1 in HCC. Treatment of cells with stable knockdown or overexpression of FMO5 with Cycloheximide (CHX) showed that FMO5 knockdown decreased the half-life of the IQGAP1 protein, while overexpressing FMO5 increased the protein half-life of IQGAP1 (Figure 8C). Furthermore, cells treated with MG132 (a proteasome inhibitor) blocked the proteasome-dependent ubiquitination degradation pathway, and the accumulation of endogenous IQGAP1 in cells overexpressing FMO5 was much higher, indicating that FMO5 inhibits the ubiquitination degradation of IQGAP1 in HCC (Figure 8D). Next, Huh7 cells co-transfection of HA-ubiquitin plasmid and Flag-IQGAP1, we analyzed the level of ubiquitination of IQGAP1. The results showed that the ubiquitination level of IQGAP1 significantly decreased in FMO5-overexpression cells, whereas in FMO5 silencing cells the ubiquitination level of IQGAP1 significantly increased (Figure 8E). The domains of IQGAP1, which move from the N to the C terminus, include a calponin homology domain (CHD domain, 44aa–159aa), a coiled-coil domain, a poly proline protein-protein domain (WW domain, 679aa–712aa), four IQ motifs that form the IQ domain (745aa–864aa), a Ras GAP-Related Domain (GRD domain, 1004aa–1237aa), and a Ras GAP C-Terminal domain (RGCT domain, 1563aa–1657aa) [27]. Thus, identification of the key domains of FMO5 that bind to IQGAP1 is essential for investigating the molecular mechanisms. Therefore,

we performed deletion mapping analyses of IQGAP1 and identified that the WW domain was the vital domain that mediates the interaction with FMO5, which fully opens the IQGAP1 structure (Figure 8F). One study demonstrated that IQGAP1 can be SUMOylated by SUMO1 at the K1445 residue, which is close to the C-terminus and stabilizes IQGAP1 by attenuating protein ubiquitination [34]. This study suggests that binding of FMO5 to IQGAP1 exposes the C-terminal K1445 site and makes it more susceptible to SUMOylation. Therefore, we examined SUMOylation of IQGAP1 during knockdown or overexpression of FMO5. Surprisingly, overexpression of FMO5 resulted in a significant increase in SUMOylation of IQGAP1 and a decrease in SUMOylation when FMO5 was knocked down (Figure 8G). Therefore, we concluded that FMO5 facilitates the SUMOylation of IQGAP1 by directly binding to it, leading to its complete structural opening, which in turn attenuates the ubiquitination degradation of IQGAP1 in HCC.

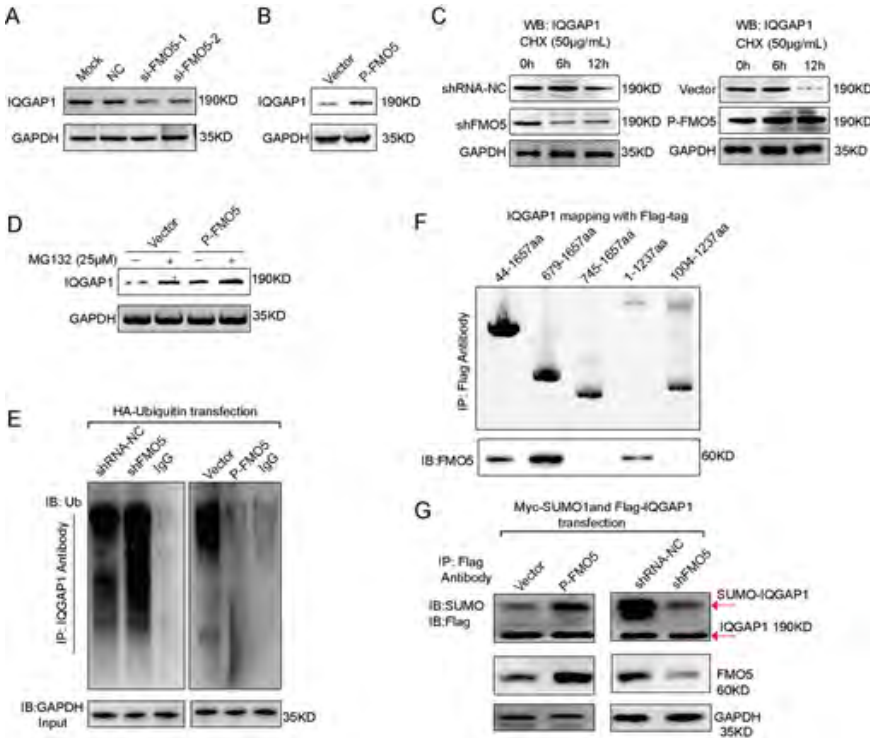

Figure 8: FMO5 blocks IQGAP1 ubiquitination by increasing its SUMOylation in HCC

(A, B): Immunoblotting for the protein level of IQGAP1in FMO5 knockdown (A) or overexpressed (B) Huh7 cells. GAPDH is the internal control. (C): Immunoblotting for the IQGAP1 levels in FMO5-knockdown cells, FMO5-overexpressed cells, or the relative control cells were treated with cycloheximide (CHX, 50 μg/ml) for the indicated times. (D): Immunoblotting of IQGAP1 level in FMO5-overexpressed cells and vector cells were treated with MG132 (25 μM) for 12 h. (E): Ubiquitination levels of IQGAP1 determined in FMO5-knockdown cells, FMO5-overexpressed cells which transfected with HA-Ubiquitin plasmids for 48h. Using the IQGAP1 antibody for IP and the ubiquitin-specific antibody for western blot. (F): Deletion mapping for the domains of IQGPA1 with flag-tag vector. Using the Flag antibody for IP and the FMO5 antibody for western blot. (G): The SUMOylated IQGAP1 was detected in the cells which co-transfection of pFlag-IQGAP1 and pMyc-SUMO1. The Flag-tagging IQGAP1 protein was enriched by IP, in which the SUMOylated IQGAP1 level was analyzed through western blot using IQGAP1 or SUMO1 antibody.

5. Discussion

The hepatic microsomal enzyme system, usually present in the endoplasmic reticulum of hepatocytes, plays a valuable role in drug metabolism in the liver [35, 36]. To date, researchers have identified a variety of metabolism-related microsomal enzyme systems including FMOs, cytochrome P450, and NADPH cytochrome c reductase [37-39]. Among them, the roles of cyP450 and NADPH cytochrome c reductase in liver metabolism have been well elucidated [40-42]. However, we believe that some enzymes that belong to the liver microsomal enzyme system are associated with the development of liver cancer.

Whole-transcriptome sequencing technology was used to analyze the differentially expressed genes in HCC tissue hepatic microsomes and further explore their roles in HCC development. After processing the sequencing data, we found that FMO5 was significantly overexpressed in sorafenib-resistant patients. The known catalysis of FMO5 is the N-oxygenation of short-chain aliphatic primary amines, such as N-octylamine, and S-oxygenation of S-methyl-esonarimod [43]. Several reports have found that interindividual differences in FMO5 expression lead to fat deposition and plasma cholesterol diversity, and that some therapeutic drug-induced FMO5 expression accelerates disease progression by affecting metabolic processes [21]. Current studies suggest that FMO5 plays an important role in liver metabolism, but its biological function in HCC remains limited.

We then analyzed the basic information of FMO5 in genomic localization, mRNA expression panel, and clinical prognosis value

of patients with HCC. Surprisingly, FMO5 is located in a region of 1q21.1 (chr1: 147,186,261–147,225,339), which we have previously identified as a significantly amplified region in HCC using the 373 cases in CNA datasets from TCGA-LIHC [16]. Several studies have shown that the copy number amplification of 1q21.1 in HCC has a significantly negative correlation with patient prognosis. To date, many oncogenes and lncRNAs with oncogenic functions have been identified in this region, suggesting a potential role for FMO5 in the progression of HCC [16, 44-46]. In vitro and in vivo assays showed that the knockdown of FMO5 significantly reduced migration, invasion, and metastasis, suggesting that FMO5 functions as an oncogene in HCC progression.

Furthermore, a GST-pulldown assay with mass spectrometry analysis confirmed that FMO5 can directly interact with IQGAP1 in HCC. IQGAP1 is the most well-characterized members of the IQGAP family, which contains several domains that mediate protein-protein interactions and thereby regulate fundamental biological processes [26]. IQGAP1 integrates signaling pathways and coordinates cellular activities, including cell migration, cell proliferation, intracellular signaling, vesicle trafficking, and cytoskeletal dynamics, which are oncogenes in several types of cancer [47-49]. IQGAP1 is modulated by several mechanisms including protein binding, self-association, subcellular localization, and phosphorylation [50, 51]. In normal cells, IQGAP1 is maintained in an inactive form that is mediated by at least two sites in the RGCT and CHD domains, and when the cells are stimulated, the interaction of N- and C-terminal halves is relieved by phosphorylation at the serine 1443 residue, and the structure of IQGAP1 is partially opened, which allows the binding of other proteins [51]. Our results show that FMO5 overexpression increases the SUMOylation of IQGAP1 at the C-terminus, which in turn decreases the ubiquitous degradation of IQGAP1 and stabilizes IQGAP1 in HCC. Thus, FMO5 acts as an oncogene by stabilizing IQGAP1 in HCC cells.

In conclusion, we identified FMO5 from hepatic microsomal enzymes in the patients' tissues. FMO5 is significantly upregulated in HCC tissues and predicts poor prognosis in patients with HCC. FMO5 has a strong correlation mRNA with IQGAP1 and this direct binding state opens the IQGAP1 structure, enhances the level of SUMOylation of IQGAP1, and decreases its ubiquitination degradation. These findings provide a new molecular target for HCC treatment, enriching the biological functions of FMO5 beyond its role as a monooxygenase. It also provides insights into potential prognosis and therapeutic targets for HCC.

6. Funding and Acknowledgements

This work was supported by grants from the National Natural Science Foundation of China (81802810), National Key Research and Development Program of China (2020YFA0113000, 2018YFA0109800), Basic Research Program of Shanghai (20JC1412200), Shanghai Municipal Health Commission (20214Y0359), and Shanghai Science and Technology Administration Commission (22Y11909100).

References

1. Sung H, Ferlay J, Siegel RZL, Laversanne M, Soerjomataram I, Jemal A, et al. Global Cancer Statistics 2020: GLOBOCAN Estimates of Incidence and Mortality Worldwide for 36 Cancers in 185 Countries. CA Cancer J Clin. 2021; 71(3): 209-49.
2. Lovet JM, Zucman-Rossi J, Pikarsky E, Sangro B, Schwartz M, Sherman M, et al. Hepatocellular carcinoma. Nat Rev Dis Primers. 2016; 2: 16018.
3. Walter P, Blobel G. Preparation of microsomal membranes for cotranslational protein translocation. Methods Enzymol. 1983; 96: 84-93.
4. Dallner G, Ernster L. Subfractionation and composition of microsomal membranes: a review. J Histochem Cytochem. 1968; 16(10): 611-32.
5. Kawajiri K, Ito A, Omura T. Subfractionation of rat liver microsomes by immunoprecipitation and immunoadsorption methods. J Biochem. 1977; 81(3): 779-89.
6. Lu Y, Cederbaum AI. Cytochrome P450s and Alcoholic Liver Disease. Curr Pharm Des. 2018; 24(14): 1502-17.
7. Uno Y, Shimizu M, Ogawa Y, Makiguchi M, Kawaguchi H, Yamato O, et al. Molecular and functional characterization of flavin-containing monooxygenases in pigs, dogs, and cats. Biochem Pharmacol. 2022; 202: 115125.
8. Poulsen LL, Masters BS, Ziegler DM. Mechanism of 2-naphthylamine oxidation catalysed by pig liver microsomes. Xenobiotica. 1976; 6(8): 481-98.
9. Poulsen LL, Ziegler DM. The liver microsomal FAD-containing monooxygenase. Spectral characterization and kinetic studies. J Biol Chem. 1979; 254(14): 6449-55.
10. Ziegler DM, Poulsen LL, McKee EM. Interaction of primary amines with a mixed-function amine oxidase isolated from pig liver microsomes. Xenobiotica. 1971; 1(4): 523-31.
11. Lawton MP, Cashman JR, Cresteil T, Dolphin CT, Elfarra AA, Hines RN, et al. A nomenclature for the mammalian flavin-containing monooxygenase gene family based on amino acid sequence identities. Arch Biochem Biophys. 1994; 308(1): 254-7.
12. Uno Y, Shimizu M, Yamazaki H. Molecular and functional characterization of flavin-containing monooxygenases in cynomolgus macaque. Biochem Pharmacol. 2013; 85(12): 1837-47.
13. Koukouritaki SB, Hines RN. Flavin-containing monooxygenase genetic polymorphism: impact on chemical metabolism and drug development. Pharmacogenomics. 2005; 6(8): 807-22.
14. Hines RN, Hopp KA, Franco J, Saeian K, Begun FP. Alternative processing of the human FMO6 gene renders transcripts incapable of encoding a functional flavin-containing monooxygenase. Mol Pharmacol. 2002; 62(2): 320-5.
15. Hernandez D, Janmohamed A, Chandan P, Phillips IR, Shephard EA. Organization and evolution of the flavin-containing monooxygenase genes of human and mouse: identification of novel gene and

pseudogene clusters. Pharmacogenetics. 2004; 14(2): 117-30.

16. Li Z, Lu X, Liu Y, Zhao J, Ma S, Yin H, et al. Gain of LINC00624 Enhances Liver Cancer Progression by Disrupting the Histone Deacetylase 6/Tripartite Motif Containing 28/Zinc Finger Protein 354C Corepressor Complex. Hepatology. 2021; 73(5): 1764-82.
17. Kong L, Chen J, Ji X, Qin Q, Yang H, Liu D, et al. Alcoholic fatty liver disease inhibited the co-expression of Fmo5 and PPARalpha to activate the NF-kappaB signaling pathway, thereby reducing liver injury via inducing gut microbiota disturbance. J Exp Clin Cancer Res. 2021; 40(1): 18.
18. Fiorentini F, Romero E, Fraaije MW, Faber K, Hall M, Mattevi A. Baeyer-Villiger Monooxygenase FMO5 as Entry Point in Drug Metabolism. ACS Chem Biol. 2017; 12(9): 2379-87.
19. Phillips IR, Shephard EA. Drug metabolism by flavin-containing monooxygenases of human and mouse. Expert Opin Drug Metab Toxicol. 2017; 13(2): 167-81.
20. Chen M, Guan B, Xu H, Yu F, Zhang T, Wu B. The Molecular Mechanism Regulating Diurnal Rhythm of Flavin-Containing Monooxygenase 5 in Mouse Liver. Drug Metab Dispos. 2019; 47(11): 1333-42.
21. Gonzalez Malagon SG, Melidoni AN, Hernandez D, Omar BA, Houseman L, Veeravalli S, et al. The phenotype of a knockout mouse identifies flavin-containing monooxygenase 5 (FMO5) as a regulator of metabolic ageing. Biochem Pharmacol. 2015; 96(3): 267-77.
22. Varshavi D, Scott FH, Varshavi D, Veeravalli S, Phillips IR, Veselkov K, et al. Metabolic Biomarkers of Ageing in C57BL/6J Wild-Type and Flavin-Containing Monooxygenase 5 (FMO5)-Knockout Mice. Front Mol Biosci. 2018; 5: 28.
23. Rizzardi AE, Johnson AT, Vogel RI, Pambuccian SE, Henriksen J, Skubitz AP, et al. Quantitative comparison of immunohistochemical staining measured by digital image analysis versus pathologist visual scoring. Diagn Pathol. 2012; 7: 42.
24. Li Z, Zhang J, Liu X, Li S, Wang Q, Di C, et al. The LINC01138 drives malignancies via activating arginine methyltransferase 5 in hepatocellular carcinoma. Nat Commun. 2018; 9(1): 1572.
25. Abel AM, Schuldt KM, Rajasekaran K, Hwang D, Riese MJ, Rao S, et al. IQGAP1: insights into the function of a molecular puppeteer. Mol Immunol. 2015; 65(2): 336-49.
26. Johnson M, Sharma M, Henderson BR. IQGAP1 regulation and roles in cancer. Cell Signal. 2009; 21(10): 1471-8.
27. Peng X, Wang T, Gao H, Yue X, Bian W, Mei J, et al. The interplay between IQGAP1 and small GTPases in cancer metastasis. Biomed Pharmacother. 2021; 135: 111243.
28. Erickson JW, Cerione RA, Hart MJ. Identification of an actin cytoskeletal complex that includes IQGAP and the Cdc42 GTPase. J Biol Chem. 1997; 272(39): 24443-7.
29. Roy M, Li Z, Sacks DB. IQGAP1 is a scaffold for mitogen-activated protein kinase signaling. Mol Cell Biol. 2005; 25(18): 7940-52.
30. Malarkannan S, Awasthi A, Rajasekaran K, Kumar P, Schuldt KM, Bartoszek A, et al. IQGAP1: a regulator of intracellular spacetime relativity. J Immunol. 2012; 188(5): 2057-63.
31. White CD, Erdemir HH, Sacks DB. IQGAP1 and its binding proteins control diverse biological functions. Cell Signal. 2012; 24(4): 826-34.
32. Rotoli D, Perez-Rodriguez ND, Morales M, Maeso MD, Avila J, Mobasheri A, et al. IQGAP1 in Podosomes/Invadosomes Is Involved in the Progression of Glioblastoma Multiforme Depending on the Tumor Status. Int J Mol Sci. 2017; 18(1).
33. Xia FD, Wang ZL, Chen HX, Huang Y, Li JD, Wang ZM, et al. Differential expression of IQGAP1/2 in Hepatocellular carcinoma and its relationship with clinical outcomes. Asian Pac J Cancer Prev. 2014; 15(12): 4951-6.
34. Liang Z, Yang Y, He Y, Yang P, Wang X, He G, et al. SUMOylation of IQGAP1 promotes the development of colorectal cancer. Cancer Lett. 2017; 411: 90-9.
35. Obach RS. Prediction of human clearance of twenty-nine drugs from hepatic microsomal intrinsic clearance data: An examination of in vitro half-life approach and nonspecific binding to microsomes. Drug Metab Dispos. 1999; 27(11): 1350-9.
36. Labuc GE, Archer MC. Esophageal and hepatic microsomal metabolism of N-nitrosomethylbenzylamine and N-nitrosodimethylamine in the rat. Cancer Res. 1982; 42(8): 3181-6.
37. Cashman JR, Zhang J. Human flavin-containing monooxygenases. Annu Rev Pharmacol Toxicol. 2006; 46: 65-100.
38. Dhuria NV, Haro B, Kapadia A, Lobo KA, Matusow B, Schleiff MA, et al. Recent developments in predicting CYP-independent metabolism. Drug Metab Rev. 2021; 53(2): 188-206.
39. Laursen T, Jensen K, Moller BL. Conformational changes of the NADPH-dependent cytochrome P450 reductase in the course of electron transfer to cytochromes P450. Biochim Biophys Acta. 2011 1814(1): 132-8.
40. Zanger UM, Schwab M. Cytochrome P450 enzymes in drug metabolism: regulation of gene expression, enzyme activities, and impact of genetic variation. Pharmacol Ther. 2013; 138(1): 103-41.
41. Hu L, Zhuo W, He YJ, Zhou HH, Fan L. Pharmacogenetics of P450 oxidoreductase: implications in drug metabolism and therapy. Pharmacogenet Genomics. 2012; 22(11): 812-9.
42. Iyanagi T, Xia C, Kim JJ. NADPH-cytochrome P450 oxidoreductase: prototypic member of the diflavin reductase family. Arch Biochem Biophys. 2012; 528(1): 72-89.
43. Hodgson E, Rose RL, Ryu DY, Falls G, Blake BL, Levi PE. Pesticide-metabolizing enzymes. Toxicol Lett. 1995; 82-83: 73-81.
44. Wong N, Chan A, Lee SW, Lam E, To KF, Lai PB, et al. Positional mapping for amplified DNA sequences on 1q21-q22 in hepatocellular carcinoma indicates candidate genes over-expression. J Hepatol. 2003; 38(3): 298-306.
45. Ma NF, Hu L, Fung JM, Xie D, Zheng BJ, Chen L, et al. Isolation and characterization of a novel oncogene, amplified in liver cancer 1, within a commonly amplified region at 1q21 in hepatocellular carcinoma. Hepatology. 2008; 47(2): 503-10.
46. Willis TG, Zalcberg IR, Coignet LJ, Wlodarska I, Stul M, Jadayel DM, et al. Molecular cloning of translocation t(1;14)(q21;q32) defines a novel gene (BCL9) at chromosome 1q21. Blood. 1998; 91(6):

1873-81.

47. Hedman AC, Li Z, Gorisse L, Parvathaneni S, Morgan CJ, Sacks DB. IQGAP1 binds AMPK and is required for maximum AMPK activation. J Biol Chem. 2021; 296: 100075.
48. Wei T, Choi S, Buehler D, Anderson RA, Lambert PF. A PI3K/AKT Scaffolding Protein, IQ Motif-Containing GTPase Associating Protein 1 (IQGAP1), Promotes Head and Neck Carcinogenesis. Clin Cancer Res. 2020; 26(1): 301-11.
49. Anakk S, Bhosale M, Schmidt VA, Johnson RL, Finegold MJ, Moore DD. Bile acids activate YAP to promote liver carcinogenesis. Cell Rep. 2013; 5(4): 1060-9.
50. Choi S, Anderson RA. IQGAP1 is a phosphoinositide effector and kinase scaffold. Adv Biol Regul. 2016; 60: 29-35.
51. White CD, Brown MD, Sacks DB. IQGAPs in cancer: a family of scaffold proteins underlying tumorigenesis. FEBS Lett. 2009; 583(12): 1817-24.